Electronic Supplementary Information

Table S1. The crystal structure and lattice parameter of MnS and FeS_2.

Material	Crystal structure	a, b, c	α, β, γ
MnS	Cubic	a=b=c=5.42 Å	α=β=γ=90°
FeS_2	Cubic	a=b=c=5.22 Å	α=β=γ=90°

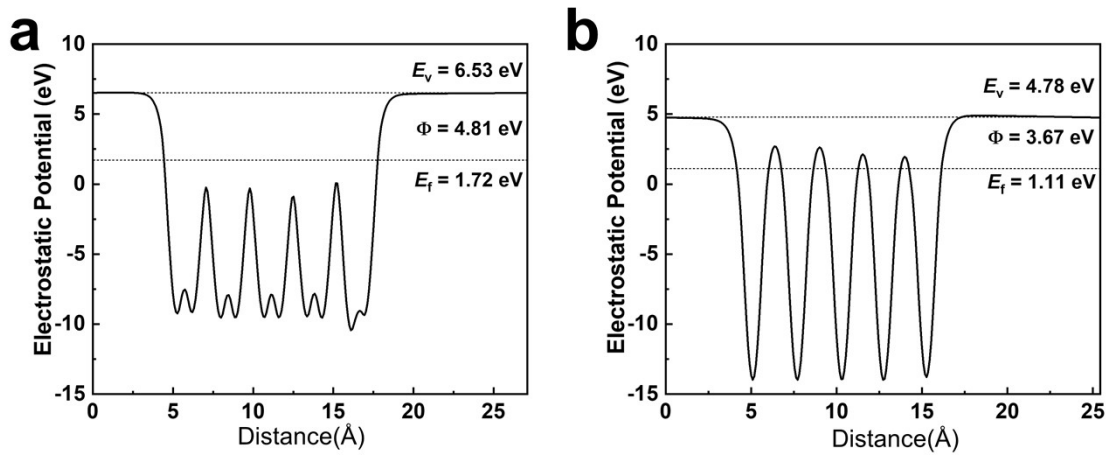

Figure S1. Calculated electrostatic potentials and work functions for a) FeS_2 (200) and b) MnS (200) surfaces.

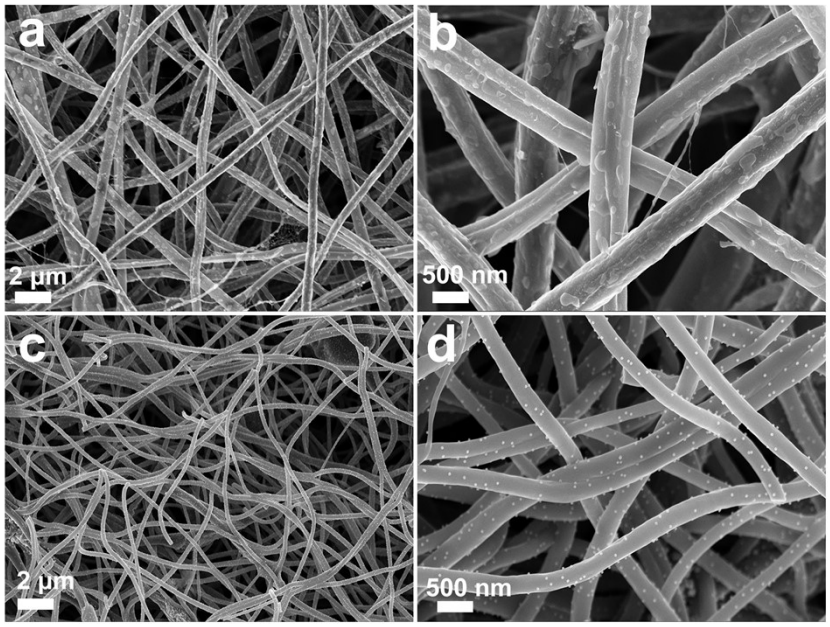

Figure S2. SEM images for (a, b) FeS_2@CNFs and (c, d) MnS@CNFs.

Table S2 ICP analysis of MnS/FeS_2@CNFs composites.

Sample	Fe (wt.%)	Mn (wt.%)	Atomic molar ratio
MnS/FeS_2@CNFs	7.49	2.64	1:0.352

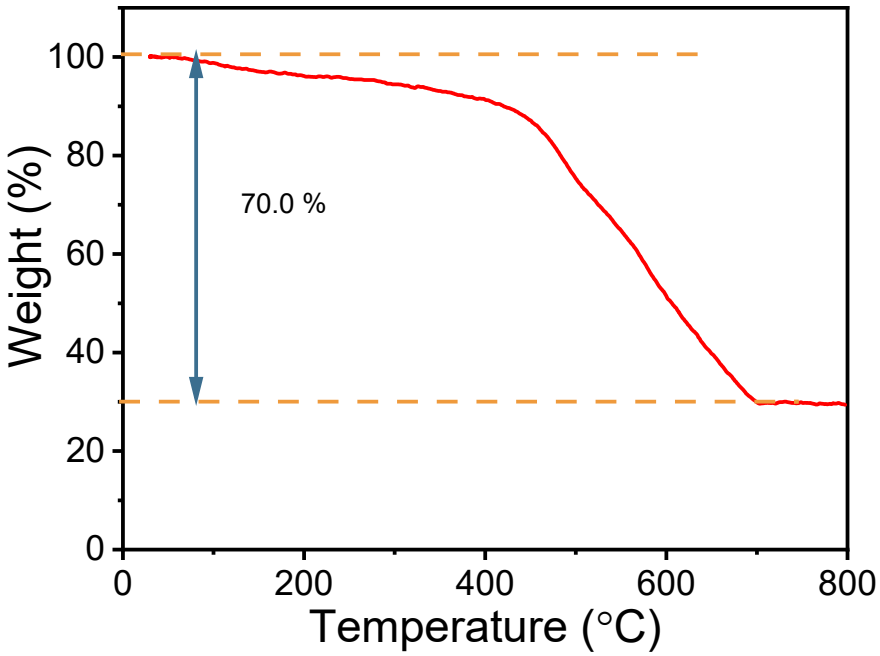

Figure S3. TG curve of MnS/FeS_2@CNFs.

TG analysis in air shows the final mass ratio of 30.0 wt% which can correspond to the stable oxidation states: Fe_2O_3 and MnO_2. According to the results of ICP, the atomic ratio of Fe and Mn in composite was approximately 1:0.352. Thus, 30.0% product includes 18.5 wt% Fe_2O_3 and 11.5 wt% MnO_2 calculated by the following equation.

$$W_{Fe_2O_3} = \frac{W_{Toal}}{0.5\,M_{Fe_2O_3} + 0.352\,M_{MnO_2}} \times 0.5\,M_{Fe_2O_3}$$

Further, 18.5 wt% Fe_2O_3 corresponds to 27.9 wt% FeS_2 according to the equation:

$$W_{FeS_2} = \frac{2 \times M_{FeS_2}}{1 \times M_{Fe_2O_3}} \times W_{Fe_2O_3}$$

Similarly, 11.5 wt% MnO_2 coincides to 11.5 wt% MnS. Then, the content of the carbon component was computed to be 60.6 wt%.

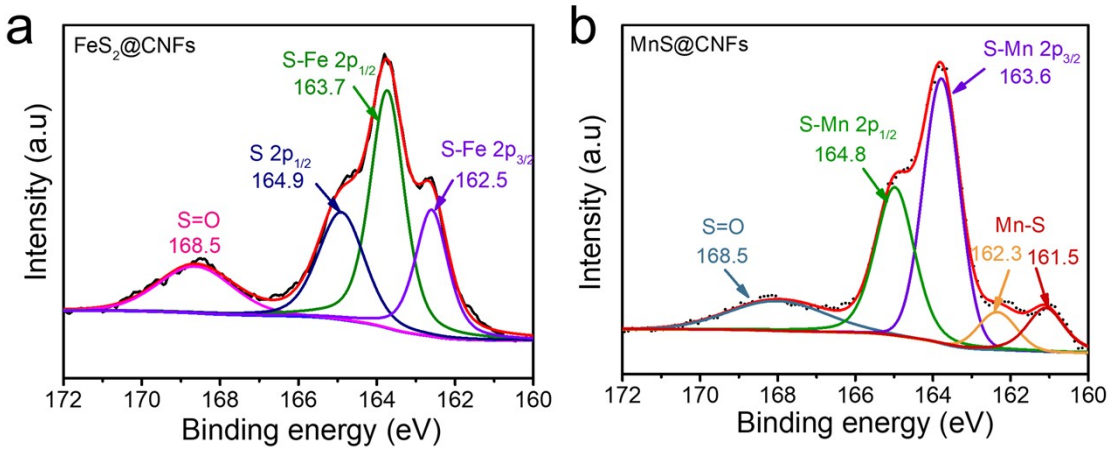

Figure S4. S 2p spectra of (a) FeS_2@CNFs and (b) MnS@CNFs.

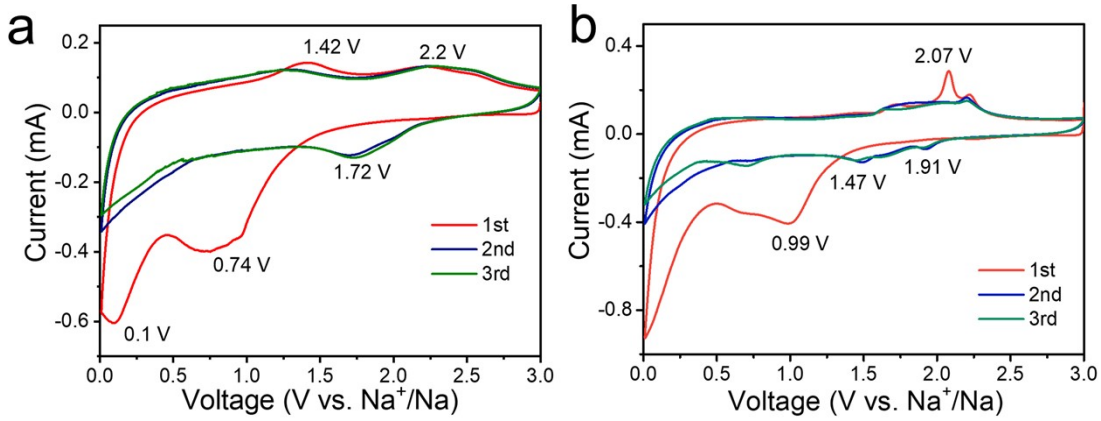

Figure S5. CV curves for the initial three cycles of (a) FeS_2@CNFs and (b) MnS@CNFs electrode at a scan rate of 0.5 mV s^{-1}.

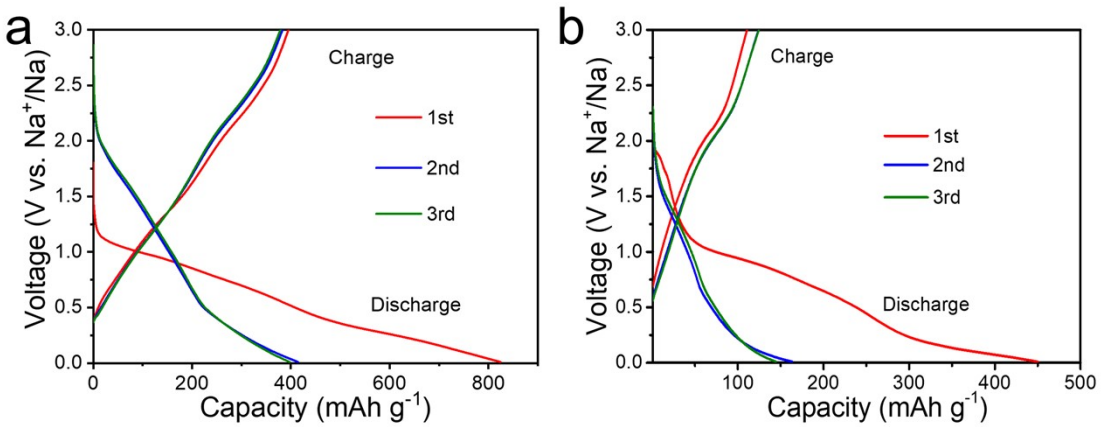

Figure S6. Galvanostatic discharge-charge curves for selected cycles of (a) FeS_2@CNFs and (b) MnS@CNFs electrode at 1.0 A g^{-1}.

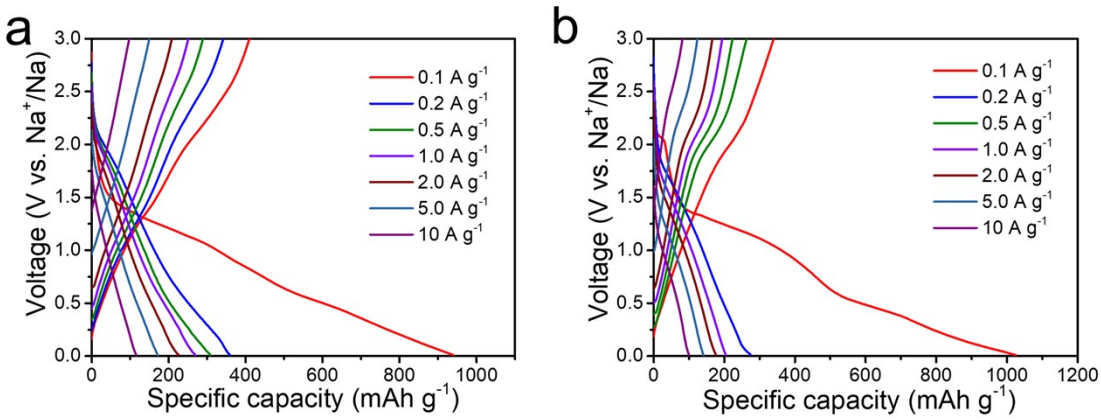

Figure S7. Galvanostatic discharge-charge curves at various current densities of (a) FeS_2@CNFs and (b) MnS@CNFs electrode.

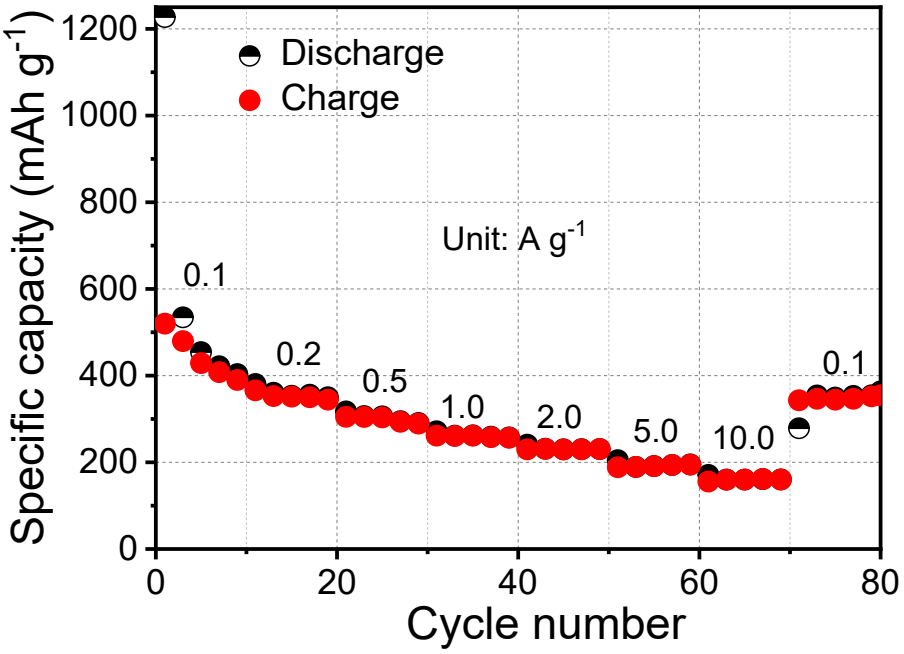

Figure S8. Rate performance of the physical mixture of MnS@CNFs and FeS_2@CNFs

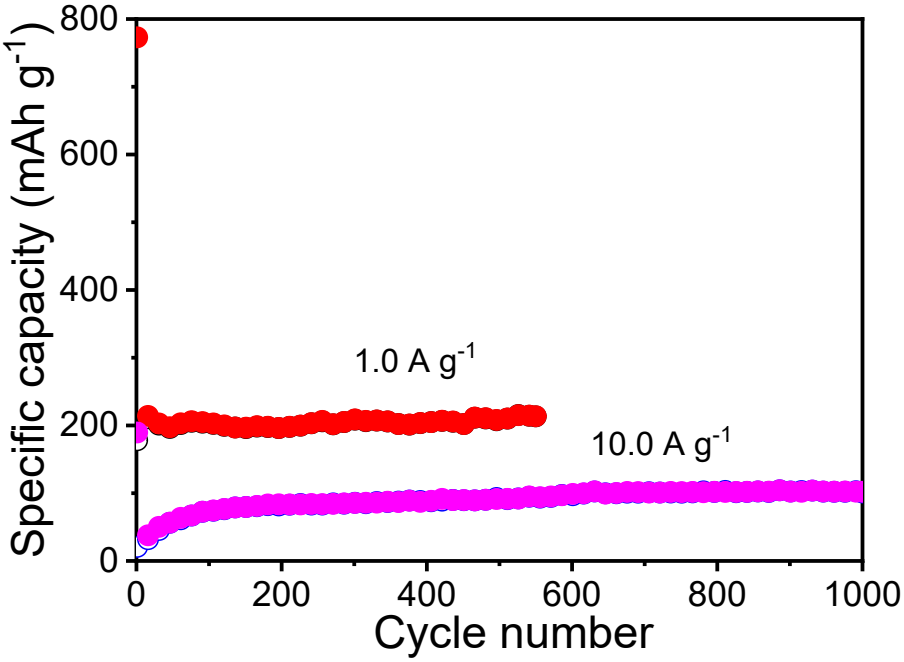

Figure S9. The cycling performance of pure CNFs under current density of 1.0 and 10.0 A g^{-1}, respectively.

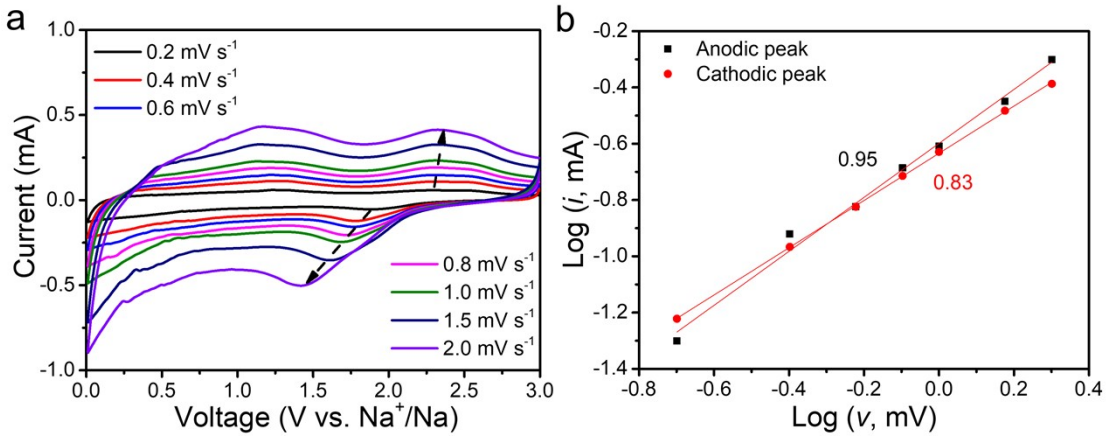

Figure S10. (a) CV curves at various scan rates and (b) *b* values at the anodic and cathodic peaks of FeS_2@CNFs electrode.

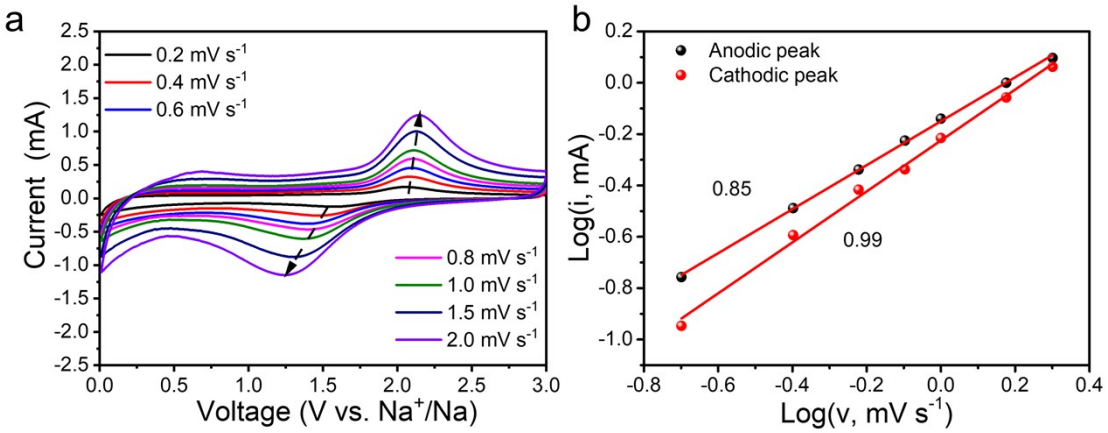

Figure S11. (a) CV curves at various scan rates and b) *b* value at the anodic and cathodic peaks of MnS@CNFs electrode.

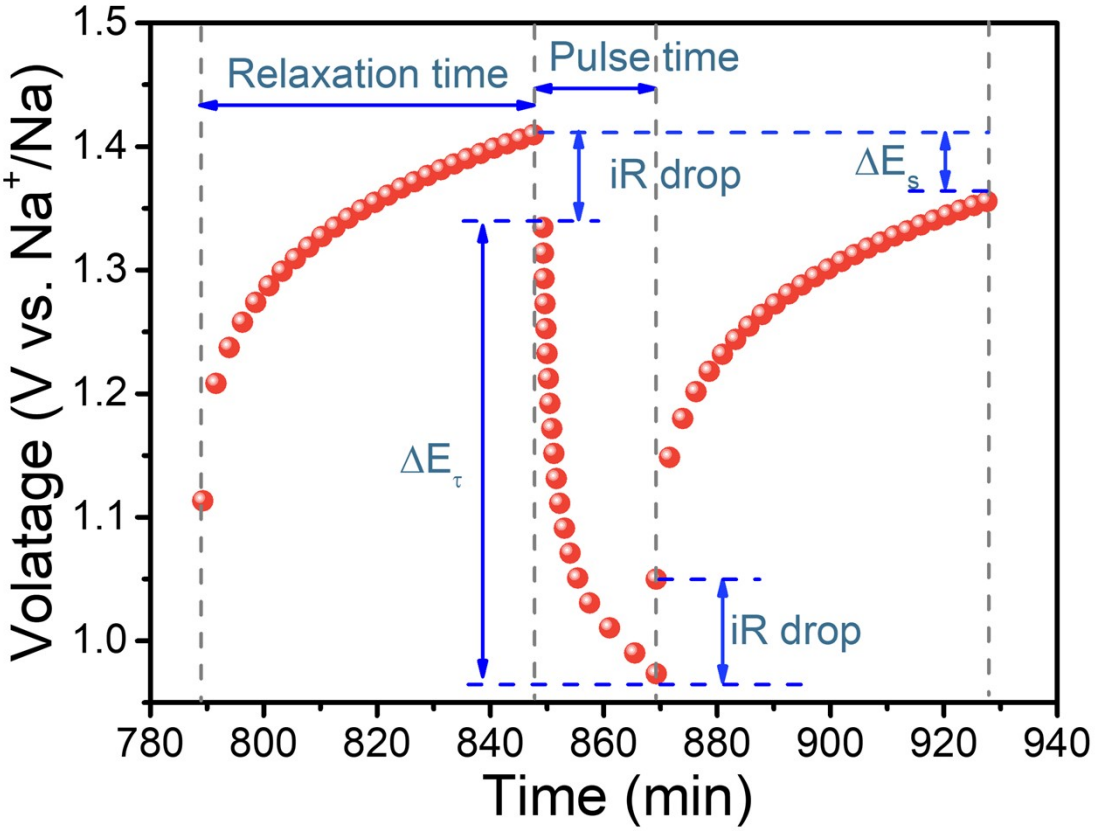

Figure S12. Discharge profiles of MnS/FeS_2@CNFs electrode for a single GITT during discharge process.

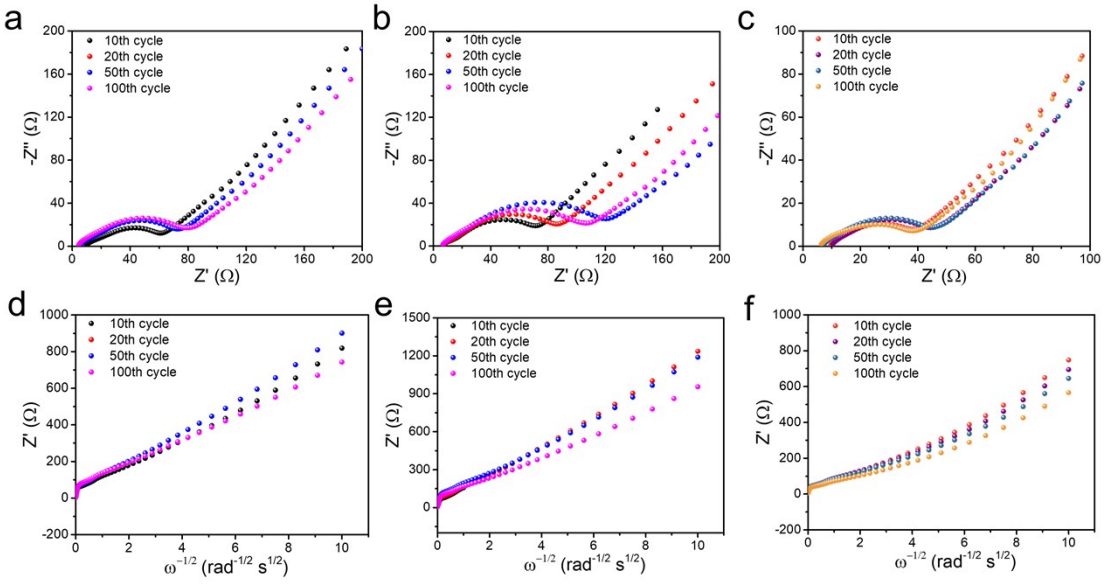

Figure S13. (a, b, c) EIS plots and (d, e, f) the relationship between Z' and w-1/2 of MnS@CNFs, FeS_2@CNFs, MnS/FeS_2@CNFs, respectively.

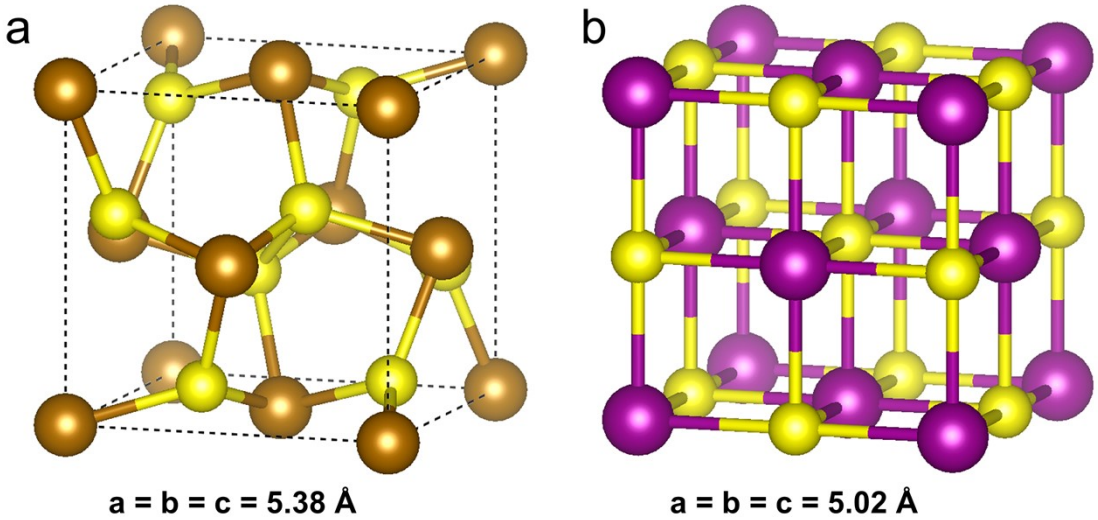

Figure S14. Optimized crystal structures of (a) FeS_2 and (b) MnS. The yellow, brown, and purple spheres denote the S, Fe, and Mn atoms, respectively.

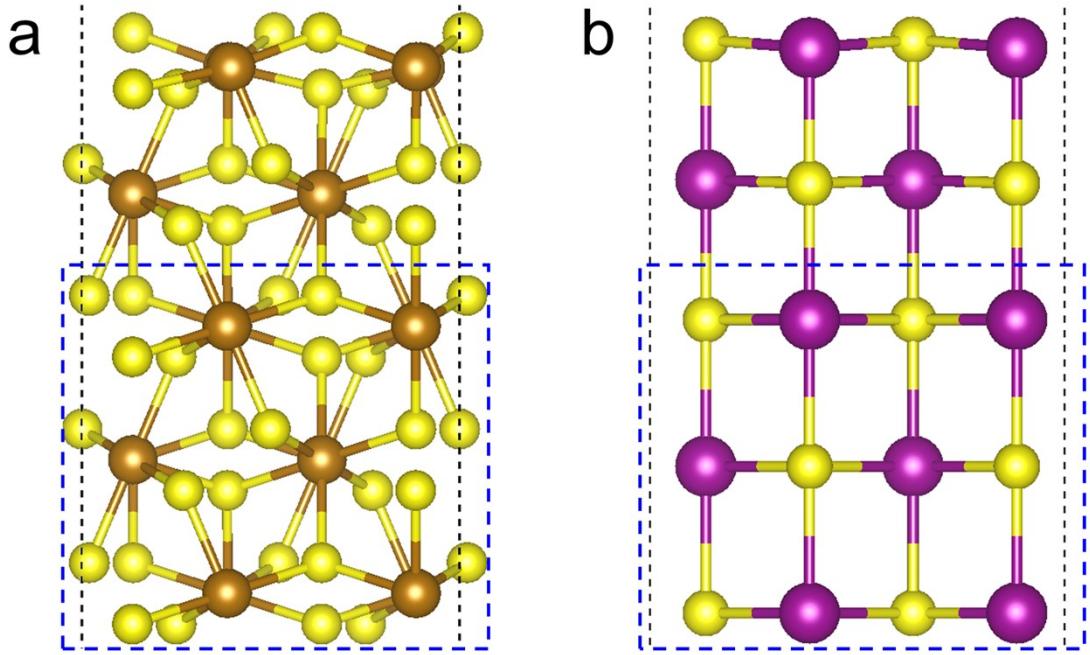

Figure S15. Slab models of the (200) surface for (a) FeS_2 and (b) MnS. The atoms in the blue box are fixed. The yellow, brown, and purple spheres denote the S, Fe, and Mn atoms, respectively.

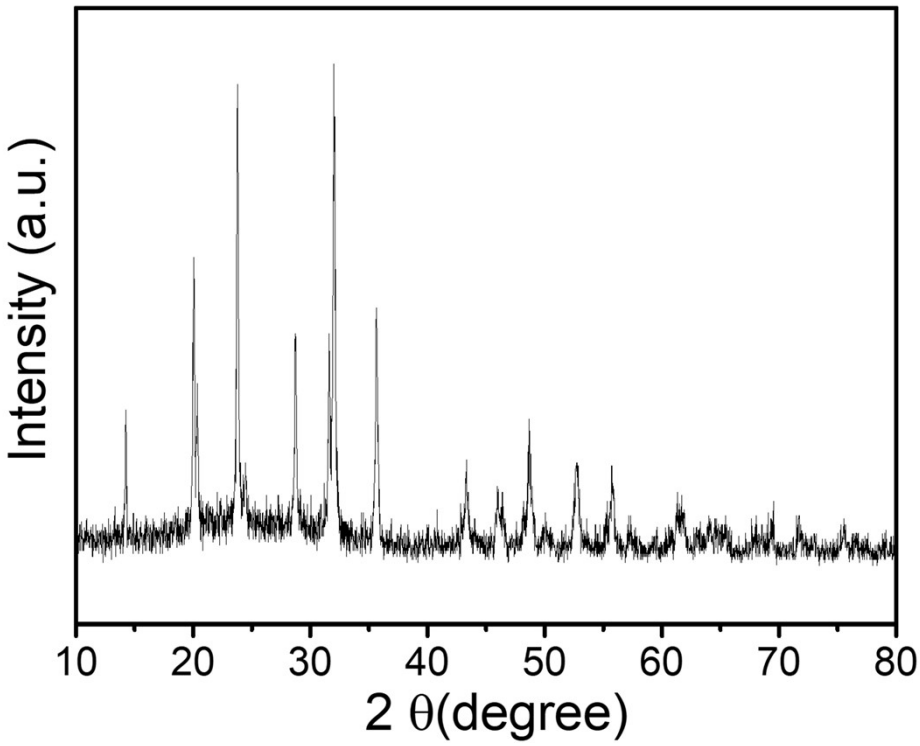

Figure S16. XRD pattern of $Na_3V_2(PO_4)_3$.

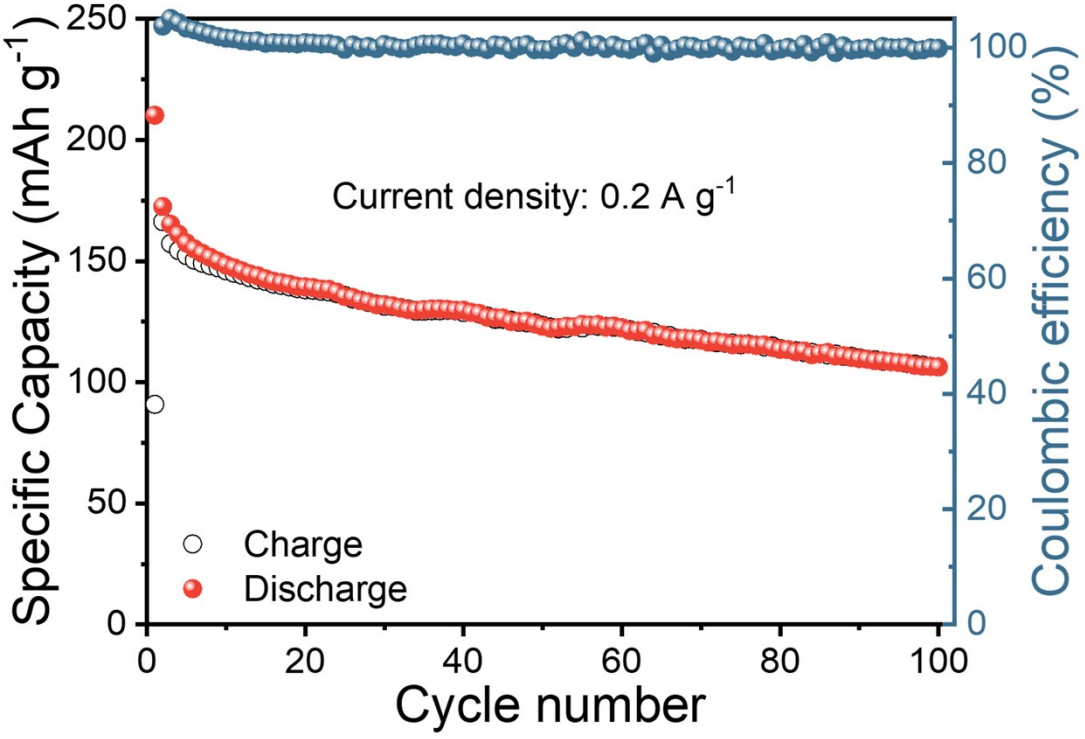

Figure S17. Cycling durability of $Na_3V_2(PO_4)_3$ cathode.

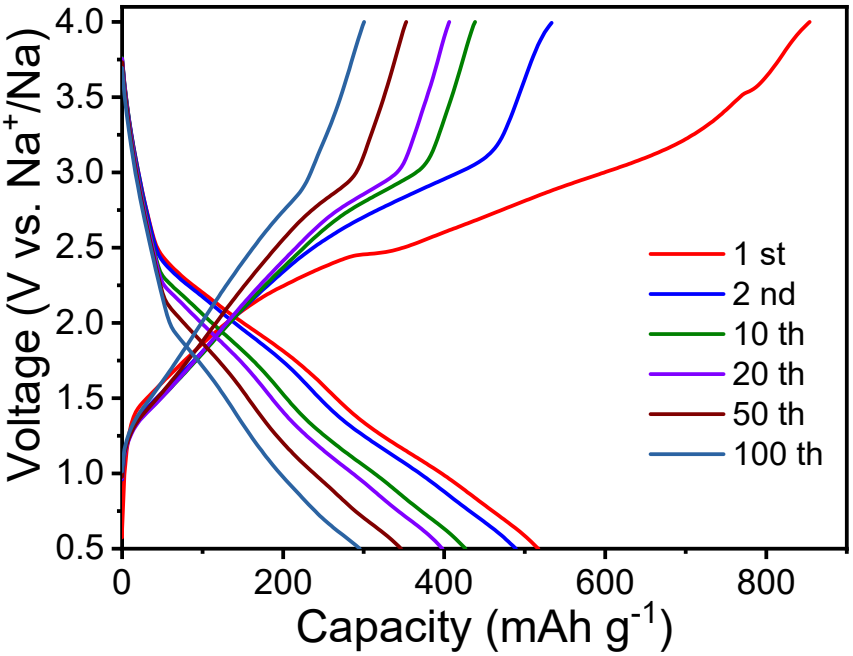

Figure S18. The charge and discharge curves of the full battery.